4.8. A Single-Inductor 0.35-µm CMOS Energy-Investing Piezoelectric Harvester

Dongwon Kwon[1,2] and Gabriel A. Rincón-Mora[1]
[1]Georgia Institute of Technology, Atlanta, Georgia
[2]Linear Technology Corporation, Milpitas, California

Because miniaturized systems store little energy, their lifespans are often short. Fortunately, vibrations are consistent and abundant in many applications, so ambient kinetic energy can be a viable source. Vibrations induce the charges in piezoelectric transducers to build electrostatic forces that damp vibrations and convert kinetic energy into the electrical domain. The shunting switches and switched-inductor circuit of bridge rectifiers in [1–2] increase this output energy by extending the damping (i.e., harvesting) duration within a vibration cycle. Because the output voltages of bridge rectifiers clamp and limit the electrical damping forces built, switched-inductor converters in [3–4], whose damping voltages can exceed their rectified outputs, draw more power from vibrations. Still, electrical–mechanical coupling factors in tiny transducers are low, so electrical damping forces (i.e., voltages) remain weak. Investing energy into the transducer can increase this force, but unlike in [5–6], which demand multiple inductors and high-voltage sources, the system presented here invests energy with only one inductor at low voltages.

The harvester proposed in Fig. 4.8.1 first waits for vibrations to charge (with i_{PZ}) the transducer's capacitance C_{PZ} to C_{PZ}'s positive peak $v_{PZ(PK)}^+$, as Fig. 4.8.2 shows. The system then invests battery energy from v_{BAT} into inductor L_H by closing switch M_P across investment time τ_I.

Afterwards, M_P opens and switch M_N closes to first harvest all C_{PZ}'s energy, which C_{PZ} accrued across the positive half cycle, into L_H during τ_H^+. M_N stays engaged after that to drain L_H's energy back into C_{PZ} until L_H's i_L nears 0 A, pre-charging C_{PZ} to $-v_{PC}$. Motion across the negative half now works against a strengthened electrical damping force (i.e., with a larger absolute value of v_{PZ}) to convert more mechanical energy into the electrical domain than without $-v_{PC}$. At the end of the negative half, M_N and M_P energize and de-energize L_H, respectively, to empty C_{PZ} into L_H and L_H into v_{BAT}, which is when v_{BAT} recovers its investment and collects all derived gains.

Since each energy transaction through L_H is much shorter than the half cycles (e.g., about 7 µs of 3.5 ms), the system can invest and harvest energy with only one inductor. The harvester builds a damping voltage that is greater than C_{PZ}'s open-circuited voltage $V_{PZ(OC)}$ and v_{BAT} not only because L_H combines the energy in C_{PZ} and v_{BAT}, but also because the amplitude of v_{BAT} does not limit how much energy L_H draws from v_{BAT}. Extending investment time τ_I increases v_{BAT}'s investment, which ultimately raises the electrical damping force with which the system draws power.

Power switches M_N and M_P in Fig. 4.8.1 are 15-V devices with a minimum channel-length of 1.5 µm that allow large voltage swings at v_{PZ} and switching node v_{SW}. After switching events, when M_P and M_N both open, switch S_{RS} in Fig. 4.8.1 shorts v_{SW} to ground to suppress undesired ringing voltages. Also, to keep parasitic p–n junctions in non-isolated NFETs in the system from engaging, off-chip sample-and-hold negative-peak detector C_{SS} and Schottky diode D_{SS} set the chip's substrate V_{SS} near v_{PZ}'s negative peak.

Driving the gate voltages of M_P (v_{GMP}) and M_N (v_{GMN}) across v_{BAT} and V_{SS}, however, demands considerable gate-drive power, so M_P and M_N drivers DRV_P and DRV_N limit gate swings to a fraction of v_{BAT}–V_{SS}. DRV_P raises v_{GMP} to v_{BAT} to disengage M_P, but only pulls v_{GMP} to 0 V to engage M_P. On the other hand, DRV_N uses flying capacitor C_F in Fig. 4.8.3 with three-state driver for M_N. Except for the two short intervals captured in the waveforms of Fig. 4.8.3, DRV_N keeps M_N off by connecting v_{GMN} to either 0 V (with S_{GND}) or v_{PZ} (with S_{PZ}), whichever voltage is lower, while charging C_F to v_{BAT}–V_{SS} through S_{PC} and S_{NC}. To engage M_N, DRV_N connects the charged C_F across v_{PZ} and v_{GMN} through S_{ND} and S_{PD}, so that M_N can secure sufficient overdrive voltage V_{DRV} even when v_{PZ} dynamically moves. Constraining M_N's gate swing this way, instead of using v_{BAT}-to-V_{SS} rails, not only reduces gate-drive losses from 24 nJ to 8 nJ but also raises v_{GMN} above v_{BAT}, when v_{PZ} peaks in the positive direction, allowing stronger overdrive than v_{BAT}.

Because R_{PK}'s voltage in Fig. 4.8.1 is positive when v_{PZ} rises and negative otherwise, comparator CP_{PK} trips when v_{PZ} begins to either fall or rise, which happens just after v_{PZ} peaks. Accordingly, when v_{PZ} reaches its positive peak, CP_{PK} closes M_P to start investing v_{BAT} energy into L_H. V_{INV} then sets how long M_P closes (via τ_I) to control how much energy v_{BAT} invests. M_N closes after that to first harvest energy in C_{PZ} into L_H during τ_H^+ (Fig. 4.8.2) and then cycle L_H's energy back into C_{PZ}, investing both v_{BAT}'s energy and C_{PZ}'s harvested energy into C_{PZ} for the negative half cycle.

The Drain Sensor, which Fig. 4.8.4 details, opens M_N when L_H drains its energy fully into C_{PZ}. During investing, L_H's i_L pulls v_{PZ} down to $-v_{PC}$. C_S samples a fraction of i_L, and M_{P0}–M_{P1} mirror the sampled current i_S into R_S so that CP_{LD} can trip when i_L nears 0 A. However, because i_L drops faster when L_H invests more energy into C_{PZ}, M_{P0}–M_{P2} mirror a small portion of i_S into C_{OS} to build an offset voltage that counters CP_{LD}'s delay and prevents CP_{LD} from tripping late – this offset is small when L_H invests little energy. 1.5 nA from the nA Generator in Fig. 4.8.1 also reduces delay by keeping the mirrors from shutting completely.

When v_{PZ} reaches its negative peak, peak detector R_{PK}–C_{PK} and CP_{PK}, whose input common-mode range need only include ground, closes M_N to harvest the energy that C_{PZ} accumulated across the negative cycle into L_H. V_{HARV} sets τ_H^-, the duration M_N engages, to a quarter of L_HC_{PZ}-resonance period. As soon as M_N disengages, i_L raises v_{SW} above v_{BAT} and CP_{CHG} detect this moment to engage M_P until the voltage that i_{BAT} produces across M_P nears 0 V.

A shaker generated the periodic vibrations from which the 2.7-cm piezoelectric cantilever, 1.8 × 1.3-mm^2 integrated circuit, and 330-µH–1.6-Ω off-chip inductor in Fig. 4.8.7 charged 475 nF. The drops of the resulting staircase voltage in Fig. 4.8.5a represent how much energy the capacitor loses after each investment. The rising step, however, is greater than the fall, so the system recovers more energy than it invests, and the gain increases with stronger vibrations and increasing investments. The harvester also drew power from aperiodic vibrations that resulted from tapping the bolt in Fig. 4.8.7. Because the impact-induced v_{PZ} is large at first but decreases rapidly, to prevent over-investments, the prototype only invests C_{PZ}'s energy and bypasses v_{BAT} investment, which is why the staircase voltage highlighted in Fig. 4.8.5b only rises. Overall, as shown in Fig. 4.8.6, the harvester produced up to 46 µW and 51 µW by investing the energy C_{PZ} accrued across the positive cycles and additional 0.8 nJ and 66 nJ from v_{BAT}, respectively.

Increasing investment raised both P_{IN} and P_O, but the gain in P_O was lesser than that of P_{IN} due to the losses in circuits. Power-conversion efficiency ($\eta = P_O/P_{IN}$) reached up to 69.2 % as the portion of investing-induced losses decreased for stronger vibrations and lesser v_{BAT} investments. The measured quiescent and gate-drive losses ranged from 0.32 to 0.63 μW and from 1.6 to 2.5 μW, respectively, across various vibration strengths and v_{BAT} investments.

Acknowledgment:

The authors thank Bryan Legates and Linear Technology for supporting this research.

References:

[1] Y.K. Ramadass and A.P. Chandrakasan, "An efficient piezoelectric energy-harvesting interface circuit using a bias-flip rectifier and shared inductor," *ISSCC Dig. Tech. Papers*, pp. 296–297, Feb. 2009.

[2] E.E. Aktakka, R.L. Peterson, and K. Najafi, "A self-supplied inertial piezoelectric energy harvester with power-management IC," *ISSCC Dig. Tech. Papers*, pp. 120–121, Feb. 2011.

[3] D. Kwon and G.A. Rincon-Mora, "A single-inductor AC–DC piezoelectric energy-harvester/battery-charger IC converting ±(0.35 to 1.2V) to (2.7 to 4.5V)," *ISSCC Dig. Tech. Papers*, pp. 494–495, Feb. 2010.

[4] T. Hehn *et al.*, "A fully autonomous pulsed synchronous charge extractor for high-voltage piezoelectric harvesters," *Proc. IEEE ESSCIRC*, pp. 371–374. Sept. 2011.

[5] M. Lallart and D. Guyomar, "Piezoelectric conversion and energy harvesting enhancement by initial energy injection," *Appl. Phys. Lett.*, vol. 97, pp. 014104-1–014104-3, 2010.

[6] J. Dicken, P.D. Mitcheson, I. Stoianov, and E.M. Yeatman, "Increased power output from piezoelectric energy harvesters by pre-biasing," *Proc. PowerMEMS*, pp. 75–78, Dec. 2009.

Captions:

Figure 4.8.1. Energy-investing switched-inductor piezoelectric harvester.

Figure 4.8.2. Measured waveforms of the piezoelectric voltage (v_{PZ}) and inductor (i_L) and battery (i_{BAT}) currents.

Figure 4.8.3. M_N's charge-pumped three-state driver DRV_N with measured waveforms.

Figure 4.8.4. L_H's energy-drain sensor.

Figure 4.8.5. Charging 475 nF from (a) periodic and (b) aperiodic vibrations.

Figure 4.8.6. Measured input (P_{IN}) and output (P_O) power and the resulting power-conversion efficiency (η) across vibration strength with different battery energy investment ($E_{I(BAT)}$).

Figure 4.8.7. Die and experimental setup photographs of the prototyped harvester.

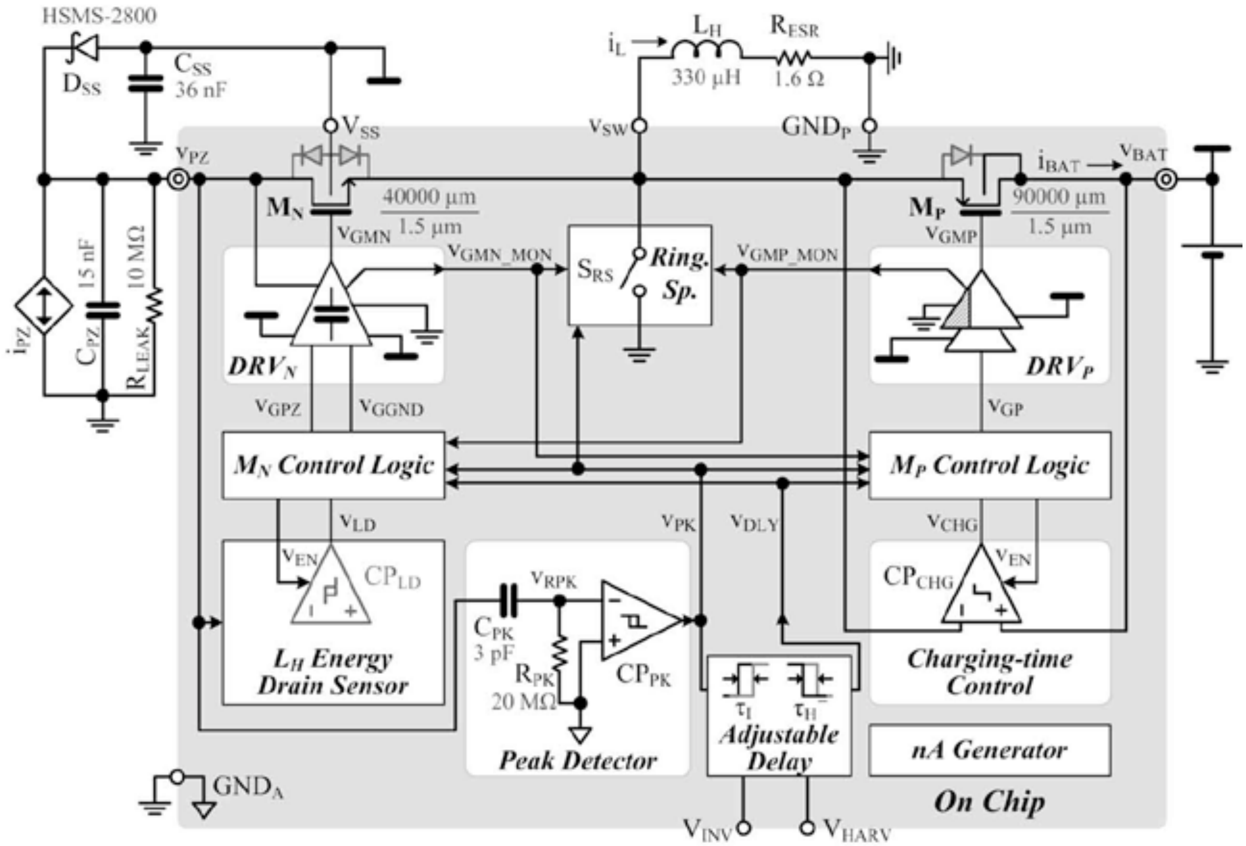

Figure 4.8.1. Energy-investing switched-inductor piezoelectric harvester.

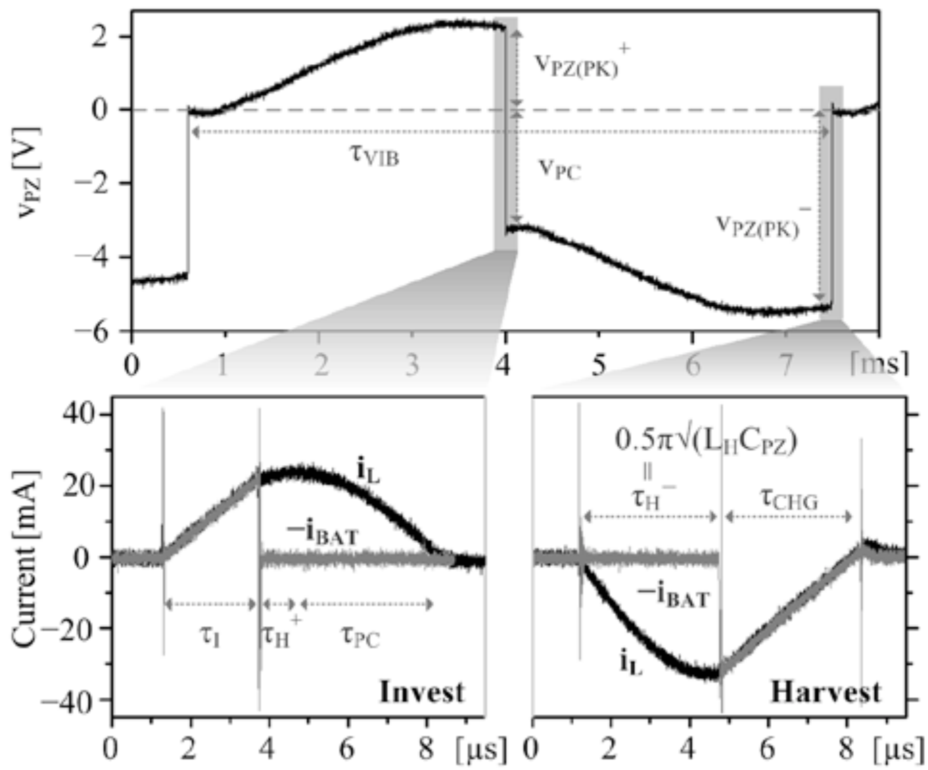

Figure 4.8.2. Measured waveforms of the piezoelectric voltage (v_{PZ}) and inductor (i_L) and battery (i_{BAT}) currents.

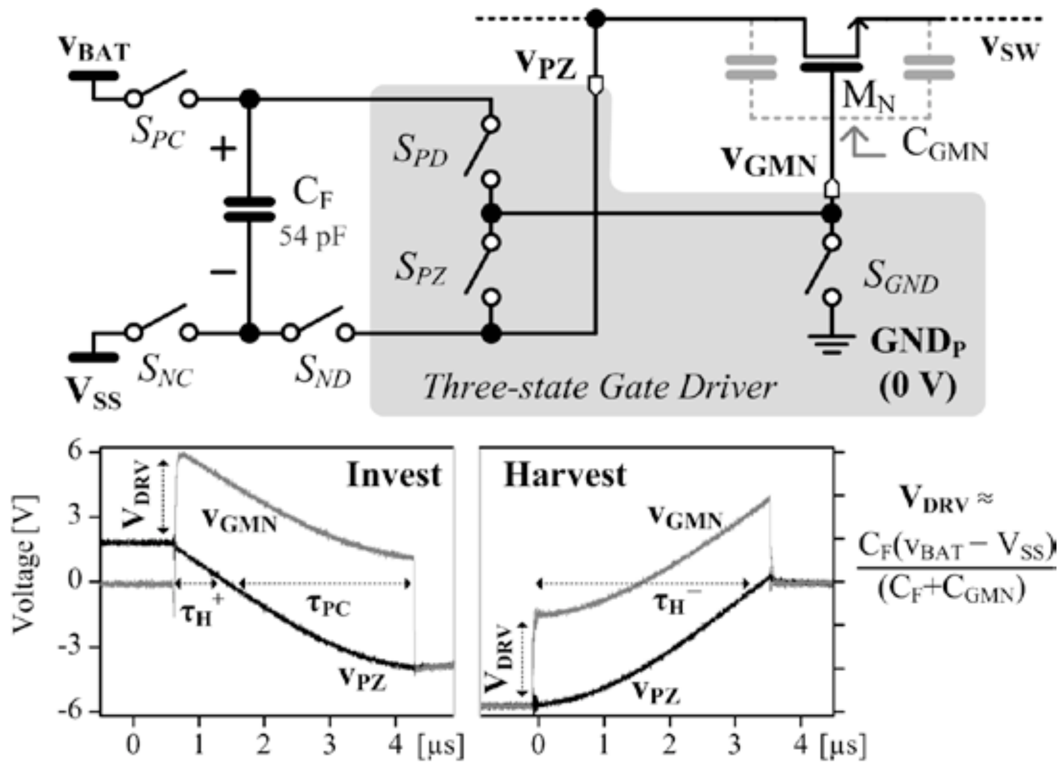

Figure 4.8.3. M_N's charge-pumped three-state driver DRV_N with measured waveforms.

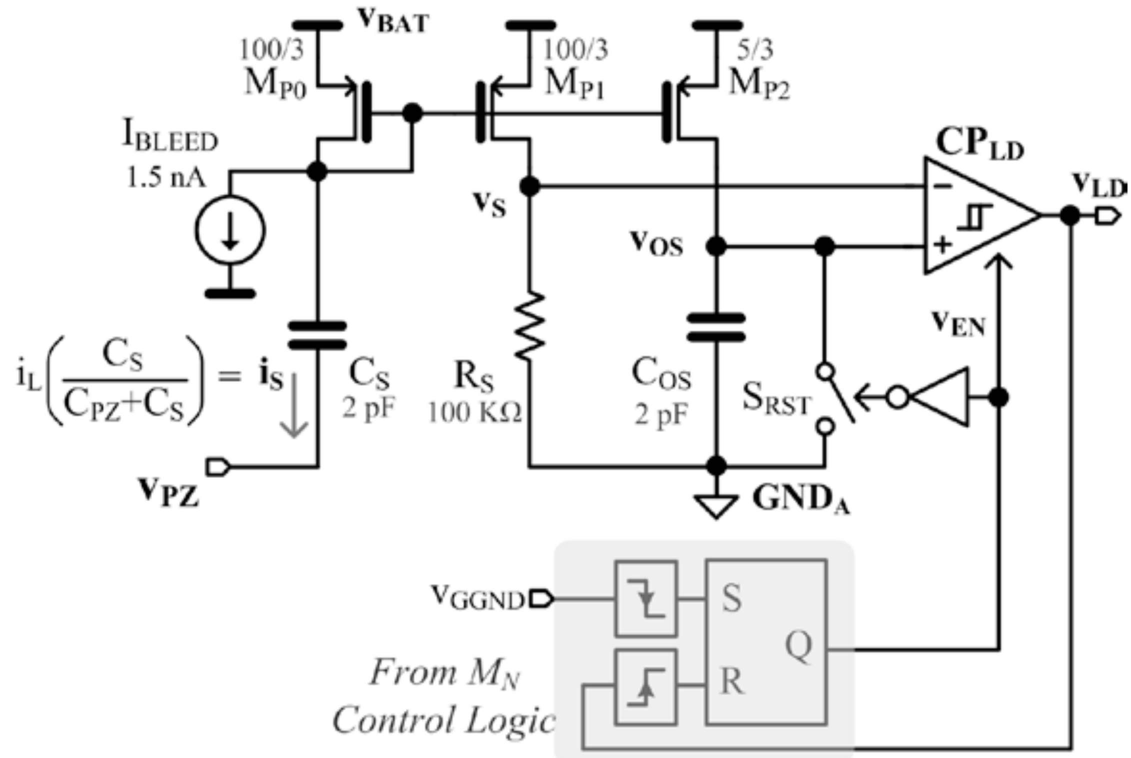

Figure 4.8.4. L_H's energy-drain sensor.

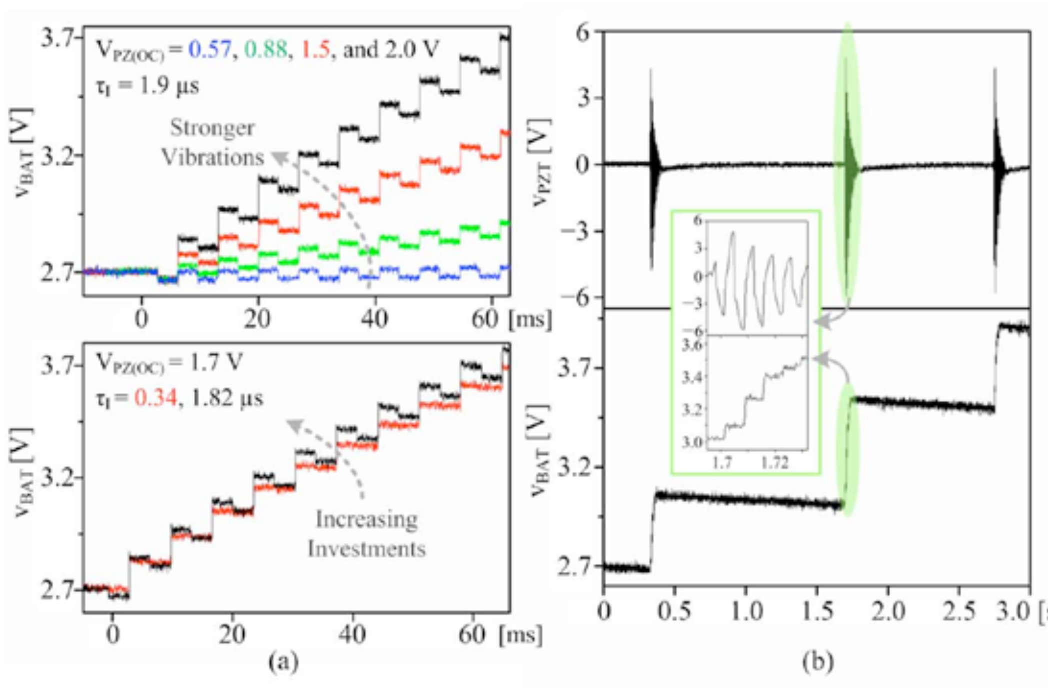

Figure 4.8.5. Charging 475 nF from (a) periodic and (b) aperiodic vibrations.

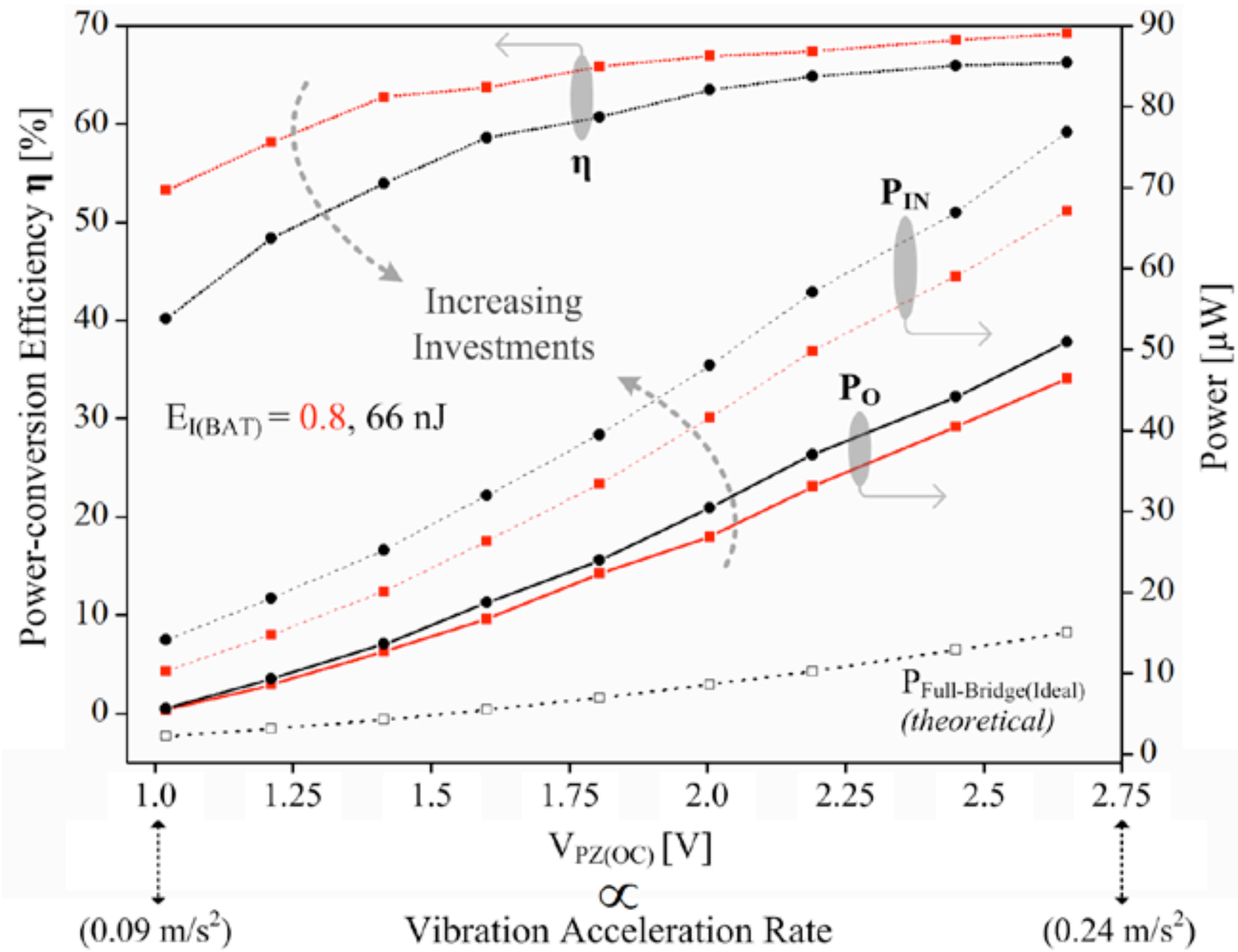

Figure 4.8.6. Measured input (P_{IN}) and output (P_O) power and the resulting power-conversion efficiency (η) across vibration strength with different battery energy investment ($E_{I(BAT)}$).

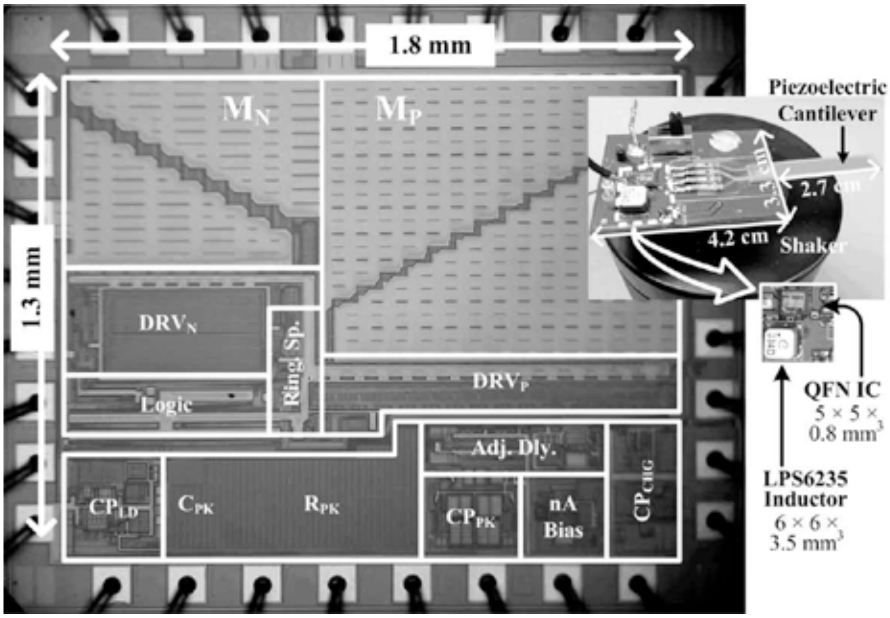

Figure 4.8.7. Die and experimental setup photographs of the prototyped harvester.